HHS Public Access

Author manuscript

Brain Stimul. Author manuscript; available in PMC 2018 January 01.

Published in final edited form as:

Brain Stimul. 2017 ; 10(1): 126–138. doi:10.1016/j.brs.2016.10.005.

Modulation of Neuronal Activity in the Motor Thalamus during GPi-DBS in the MPTP Nonhuman Primate Model of Parkinson's Disease

Abirami Muralidharan[a,1], **Jianyu Zhang**[a], **Debabrata Ghosh**[b,2], **Mathew D. Johnson**[c], **Kenneth B. Baker**[a], and **Jerrold L. Vitek**[a,*]

[a] Department of Neurology, University of Minnesota, Minneapolis, MN 55455, USA

[b]Cleveland Clinic, Cleveland, OH 44195, USA

[c] Department of Biomedical Engineering, University of Minnesota, Minneapolis, MN 55455, USA

Abstract

Background—The motor thalamus is a key nodal point in the pallidothalamocortical "motor" circuit, which has been implicated in the pathogenesis of Parkinson's disease (PD) and other movement disorders. Although a critical structure in the motor circuit, the role of the motor thalamus in mediating the therapeutic effects of deep brain stimulation (DBS) of the internal segment of the globus pallidus (GPi) is not fully understood.

Objective—To characterize the changes in neuronal activity in the pallidal (ventralis lateralis pars oralis (VLo) and ventralis anterior (VA)) and cerebellar (ventralis posterior lateralis pars oralis (VPLo)) receiving areas of the motor thalamus during therapeutic GPi DBS.

Methods—Neuronal activity from the VA/VLo (n = 134) and VPLo (n = 129) was recorded from two non-human primates made parkinsonian using the neurotoxin 1-methyl-4-phenyl-1,2,3,6-tetrahydropyridine. For each isolated unit, one minute of data was recorded before, during and after DBS; a pulse width of 90 μs and a frequency of 135 Hz were used for DBS to replicate commonly used clinical settings. Stimulation amplitude was determined based on the parameters required to improve motor signs. Severity of motor signs was assessed using the UPDRS modified for nonhuman primates. Discharge rate, presence and characteristics of bursts, and oscillatory activity were computed and compared across conditions (pre-, during, and post-stimulation).

Results—Neurons in both the pallidal and cerebellar receiving areas demonstrated significant changes in their pattern of activity during therapeutic GPi DBS. A majority of the neurons in each nucleus were inhibited during DBS (VA/VLo: 47% and VPLo: 49%), while a smaller subset was excited (VA/VLo: 21% and VPLo: 17%). Bursts changed in structure, becoming longer in duration and both intra-burst and inter-spike intervals and variability were increased in both subnuclei. High frequency oscillatory activity was significantly increased during stimulation with 33% of

* Corresponding author. Fax: 612-625-7950. vitek004@umn.edu (J.L. Vitek).
[1]Present address: Second Sight Medical Products, Building 3, 12744 San Fernando Road, Sylmar, CA 91342.
[2]Present address: Neurology and Pediatrics, Nationwide Children's Hospital, Ohio State University Medical Center, 700 Children's Drive, Columbus, Ohio 43205.

VA/VLo (likelihood ratio: $p < 0.0001$) and 34% of VPLo ($p < 0.0001$) neurons entrained to the stimulation pulse train.

Conclusions—Therapeutic GPi DBS produced a significant change in neuronal activity in both pallidal and cerebellar receiving areas of the motor thalamus. DBS suppressed activity in the majority of neurons, changed the structure of bursting activity and locked the neuronal response of one-third of cells to the stimulation pulse, leading to an increase in the power of gamma oscillations. These data support the hypothesis that stimulation activates output from the stimulated structure and that GPi DBS produces network-wide changes in neuronal activity that includes both the pallidal and cerebellar thalamo-cortical circuits.

Keywords

DBS; GPi; Non-human primate; Parkinson's disease; Motor thalamus

Introduction

Parkinson's disease (PD) is a debilitating, neurodegenerative disorder marked by a progressive loss of dopaminergic neurons in the substantia nigra pars compacta (SNc) resulting in a reduction in dopamine levels throughout the basal ganglia. The mechanistic link between these anatomical changes and the development of the cardinal motor features of PD (e.g., rigidity, tremor and bradykinesia/akinesia) remains elusive. This uncertainty regarding the physiological changes underlying parkinsonian motor signs has also led to debate over the mechanisms of the therapeutic effects of deep brain stimulation (DBS) in the subthalamic nucleus (STN) or internal segment of the globus pallidus (GPi).

Although alleviation of motor signs during high frequency stimulation of either structure is well documented [1,2], most studies report the effect of deep brain stimulation (DBS) at the site of stimulation with few studies characterizing the effect of DBS on the activity of sites to which these areas project. Studies examining the downstream effects of GPi DBS on the motor thalamus have been limited, and include work performed in normal animals [3] and a pair of single-case studies performed intra-operatively in patients with dystonia [4,5]. The purpose of this study was to investigate, in the awake, non-human primate model of parkinsonism, the effect of therapeutic, high frequency GPi stimulation on neuronal activity in the cerebellar (ventralis posterior lateralis pars oralis – VPLo) and pallidal (ventralis lateralis pars oralis – VLo and ventralis anterior – VA) receiving areas of the motor thalamus, key nodal points in the pallidothalamocortical motor circuit [6]. Comparison of the results of the present study to those observed previously by our group during STN DBS [7] revealed clear differences in the pattern and time course of GPi DBS effects on thalamic neuronal activity and could account for temporal differences observed in the relative effect of stimulation in the STN and GPi on the motor signs of PD.

Methods

All surgical and behavioral procedures were performed under protocols approved by the Institutional Animal Care and Use Committee and complied with United States Public

Health Service policy on the humane care and use of laboratory animals. Two female rhesus macaques (*M. mulatta*, ≈5.0 kg), N (9 y.o.) and S (13 y.o.), were used for this study.

Cephalic chamber placement

Pre-operative cranial CT and 7-T volumetric MRI were acquired and merged using the Cicerone software package [8] to facilitate surgical planning for cephalic chamber placement. The recording hardware was implanted in an aseptic surgical procedure under isoflurane anesthesia, the details of which have been reported previously [7,9]. In brief, following sedation and surgical preparation the head was secured in a stereotaxic frame (Kopf Instruments, Tujunga, CA, USA), the scalp was incised at the midline, and partial blunt dissection of the skin and temporal muscle was performed bilaterally. Two craniotomies were created under stereotactic guidance leaving the dura intact. The first chamber was positioned and aligned to allow for targeting of the motor thalamus and GPi while the second was located over the primary motor cortex. A series of titanium screws were placed across the exposed calvarium to reinforce the implant. Once the cephalic chambers were in place, the chambers, screws and a head restraint post were encased in dental acrylic. Post-surgically, animals were provided ad libitum food and water access for a minimum of two weeks. Buprenorphine was administered prophylactically for pain management (0.01–0.03 mg/kg I.M BID for 2 days then PRN) in combination with Metacam (0.2–0.3 PO every 24 hours on days 2–4). Prophylactic antibiotics were given preoperatively and continued postoperatively for 7–10 days.

Induction of the parkinsonian state

Each animal was made parkinsonian by one or more intracarotid injections of the neurotoxin 1-methyl-4-phenyl-1,2,3,6 tetrahydropyridine (MPTP – 0.1% solution in saline). Additional systemic injections were given intramuscularly to titrate the animal's level of severity and to maintain a stable, asymmetric parkinsonian model. The total dose of MPTP administered was similar for the two animals at 26 and 28 mg (N and S, respectively).

Behavior and clinical assessments

Bradykinesia was assessed using a modified, three-well Klüver board task. Each well was baited with a small food reward and trials were initiated upon removal of an opaque panel between the animal and the wells. Trials were videotaped and digitized at a rate of 30 frames per second for off-line analysis. Three separate behavioral epochs (i.e., reach, manipulation and retrieval time) were examined. Reach time was defined as the duration of time between the animal's hand leaving its mouth and its arrival at the plane of the Klüver board; manipulation time was calculated as the time that the animal's hand was located over the plane of the Klüver board; and retrieval time was defined as the duration of time between the animal's hand leaving the board and arriving at the mouth. Since reach time was defined as the time to reach the Klüver board from the primate's mouth, the initial reach of each trial, which began with the animal's arm at rest on the primate chair, was excluded. As the behavioral data were not normally distributed, the Wilcoxon rank-sum test (χ^2(DoF, N)) was used to compare movement times between the ON and OFF DBS conditions.

Overall motor severity was characterized using a version of the Unified Parkinson's Disease Rating Scale [10] modified (mUPDRS) for use in non-human primates; the investigator assessing the subject was not blinded to the treatment condition (i.e. DBS ON/OFF). The overall rating represents the sum of scores across 10 subscales including: posture, gait, balance, turning, defense reaction, rigidity, bradykinesia, akinesia, tremor and food-retrieval, where each item is rated from 0 to 3; although food retrieval is a part of the mUPDRS, we only assessed the cardinal motor symptoms of rigidity, tremor, akinesia and bradykinesia. Since we use a predominantly hemi-parkinsonian model in this study, the left and the right sides were assessed separately for the appendicular symptoms and we report the scores for the side contralateral to the MPTP injections in this report; hence, the maximum possible mUPDRS scores for the appendicular and axial symptoms are 24 and 15 respectively. Assessment of the mUPDRS was done on the day of, but prior to the microelectrode recordings; the Klüver board task was not done on the same day as the microelectrode recording. The animal's head was restrained during both tasks. The animal was first assessed with stimulation turned OFF and then with DBS ON; stimulation was continuously ON during the behavioral assessments in the DBS ON condition. Assessments were used to define the level of motor severity achieved following MPTP exposure, to ensure stability of the parkinsonian state across the experimental period, and to characterize the therapeutic benefit of GPi DBS. The OFF DBS and ON DBS scores were compared using Fisher's exact test.

Electrophysiology

Once a stable, moderately parkinsonian state was achieved, defined as a total mUPDRS score between 15 and 28, sensorimotor GPi was identified using serial extracellular microelectrode mapping techniques similar to those applied during human functional neurosurgery [11]. The implant procedure has been described in detail by Elder et al. [12]. Briefly, the animals were seated comfortably, with their head restrained. A tungsten micro-electrode was advanced using the Narishige micro-drive, attached to the cephalic chamber targeting the pallidum. For each unit that was isolated, the receptive field was identified by passive manipulation of the joints of the arms and legs and palpating the muscles of the face. Once the sensorimotor GPi was identified, a scaled version of the DBS lead used in humans, consisting of four (monkey N) or eight (monkey S) concentric ring platinum–iridium contacts with a diameter of 0.76 mm, a height of 0.50 mm and inter-contact spacing of 0.50 mm, was implanted. The animal was anesthetized during the DBS lead implant.

In monkey N, the IPG was implanted in the back, between the shoulder blades. The wires from the IPG were tunneled up through the neck and attached to the wires from the DBS lead. In monkey S, the wires from the DBS lead were tunneled into a dry chamber with no open craniotomy, and the IPG was attached to the wires acutely for each recording session. In both cases, the wires from the lead and IPG (monkey N only) were covered with dental acrylic to avoid damage. Stimulation was turned on/off during recording or behavior testing using the programmer (Model 7424, Medtronic Inc.) with stimulus frequency and pulse width fixed at 135 Hz and 90 μs, respectively.

Once the animal had recovered from the DBS lead implant (~2 weeks), each contact of the DBS lead was evaluated independently for its effect on parkinsonian motor signs and side-effect profile (e.g., muscle contraction), with amplitude (constant-voltage) titrated in a step-wise fashion. Those parameters yielding the greatest improvement in motor signs at the lowest stimulation amplitude were used throughout the remainder of the study; the stimulation currents for monkey N and monkey S were 1.7 and 1.3 mA, respectively.

During recording sessions the animal was seated in a primate chair with its head restrained. Tungsten microelectrodes (impedance 0.5–1.0 MΩ at 1 kHz) were advanced by a micro-drive attached to the recording chamber (Alpha Omega, Nazareth Illit, Israel). The thalamic recording chamber was oriented such that the microelectrode penetrations were made in the sagittal plane at approximately 25° from vertical. As the microelectrode was advanced, the acoustically transduced neuronal activity was monitored, with qualitative correlations between spontaneous movements or passive manipulation of the limbs used to characterize the receptive field of each isolated neuron. In addition, micro-stimulation (constant current: 10–40 μA), using the recording electrode, was performed to differentiate between pallidal and cerebellar receiving sites as reported previously [13,14]; micro-stimulation in VPLo evoked movement about the limbs at low current thresholds (10–40 μamps). Stimulation of VA/VLo neurons either does not evoke a response or does so only at high current amplitudes; likely due to current spread to VPLo given these typically occur near the border between VPLo and VLo. Spontaneous neuronal activity was recorded for 1 minute each before (pre-DBS), during and after (post-DBS) therapeutic GPi DBS. Neuronal activity was acquired using a Spike 2 data acquisition system from animal N (band pass filter 0.1–10 kHz, sampling rate 100 kHz) and using an Alpha Omega system from animal S (band pass filter 0.3–6 kHz, sampling rate 25 kHz). The filtered analog signals were sampled and stored on a computer hard disk for offline analysis. During recording sessions the animals were continuously monitored during the time the activity of the isolated units was being recorded. In addition, the receptive field of each isolated unit was determined by manipulating the animals' limbs and palpating its facial muscles. The continuous monitoring and frequent interactions with the animals insured that they were in an awake and alert state during the recording period.

Off-line analysis of single unit activity

Stimulation artifacts were removed from the digitized signal using template-based subtraction algorithms similar to those described previously [15]; an example of microelectrode recording before and after artifact subtraction is shown in Fig. 1A. A blanking pulse was applied during the phase of the stimulation artifact that saturated the recording amplifier. Since this could potentially result in the loss of action potentials during the DBS phase, simulated blanking pulses were also applied at the same frequency to the pre- and post-DBS samples to equalize the probability of spikes being lost to chance overlap. Action potentials were discriminated from the processed signal using a combination of principal component and template matching techniques, assuming a minimum refractory period of 1.0 ms (Offline Sorter, Plexon Inc., Plano, TX). The sequence of action potential and stimulation timestamps were stored for further analysis.

Post-stimulus time histograms (PSTH) of neuronal activity before, during and after stimulation were constructed by aligning the occurrence of action potentials with the onset of each DBS pulse at 0.2 ms intervals; pseudo pulses at 135 Hz were generated to allow for similar alignment within the pre- and post-DBS epochs (Fig. 1B). Action potentials that occurred in the first 0.6 ms after each DBS pulse were excluded. The discharge rate within each bin of the PSTH during stimulation was assessed for a significant increase or decrease as described previously [16]. Briefly, the mean of the pre-stimulation PSTH was subtracted from the PSTH for the DBS and post-stimulation intervals. The area under the curve for each continuous section bounded by the zero line and the PSTH curve (shaded black, red, and blue in Fig. 1B i–iii) was calculated for the pre-, during-and post-DBS PSTHs using trapezoidal numerical integration. The threshold for detecting significant changes during- and post-DBS was set as mean plus three standard deviations (dotted line in Fig. 1C) of the area under the curve(s) for the pre-DBS interval (sections shaded black in Fig. 1Bi and the black squares in Fig. 1C). The response of each neuron was then categorized as excitation (E), excitation-inhibition (EI), inhibition (I), inhibition-excitation (IE) or no-change (NC) depending on the number, duration and polarity of significant changes as illustrated in Fig. 1D. The neurons were further classified as exhibiting a tonic, bi- or poly-phasic response. Differences in average discharge rate between the three phases were examined using the paired t-test (t(DoF)). All significance thresholds were Bonferroni corrected for multiple comparisons.

Burst activity of each neuron was examined using the modified Poisson surprise algorithm [17]. This algorithm identifies bursts as low probability events assuming that the spike times within a train of action potentials have a Poisson distribution. The minimum inter-spike interval for detecting bursts in all three phases was set to half the average inter-spike interval during the pre-DBS interval. The minimum number of spikes in a burst was set as two and the maximum as ten [17]. Any group of spikes, defined as a burst by the algorithm, with a p value less than or equal to 0.05 (surprise index ≥ 3.0) was considered significant. For each unit, the frequency of bursting (bursts per min), mean intra-burst rate (IBR, spikes/s), burst duration, the percent of spikes within bursts, and the median and inter-quartile range of the intra-burst, inter-spike interval were calculated during the pre-, during- and post-DBS intervals. Differences in the percent of cells with burst activity between the three phases were identified using the Likelihood ratio test (χ^2(DoF, N)). Two-tailed, paired t test (t(DoF)) was used to test for differences in bursting activity between the three intervals. The presence of a significant effect of the type of response to DBS and burst activity during the post-DBS phase was examined using the Kruskal–Wallis test (K(DoF,N)) and post-hoc multiple comparison using the Wilcoxon rank sum test (z(DoF)).

The presence of oscillatory activity in the spike train was quantified by the multi-taper method [18]. Spike timestamps were binned into two millisecond intervals to create the rate histogram. Three orthogonal tapers were applied to non-overlapping four-second segments and the resulting power spectra were averaged. This process yields power spectral density estimates at a resolution of 0.24 Hz in the 0–200 Hz range. The threshold for detection of significant peaks in the 0.5–150 Hz range was set as three standard deviations above the mean power of the spectrum in the same range; a spectral peak was considered significant only if two consecutive bins crossed the threshold. The 0.5–150 Hz frequency range was

divided into bands: 0.5–3 Hz, 3–8 Hz, 8–13 Hz, 13–20 Hz, 20–30 Hz, 30–58 Hz, 65–90 Hz and 90–150 Hz; the left side limits of each band were excluded from the band. Distortion of the spectra due to the refractoriness of the cell was corrected using the local-shuffling method [19]. The corrected spectrum is the ratio of the original and normalizing spectrum; the normalizing spectrum was calculated from the same spike train, but after shuffling spikes with inter-spike intervals less than 500 milliseconds; the shuffling was repeated 100 times and the normalizing spectrum is the average of the power spectral density calculated from the shuffled spikes. Difference in the proportion of cells with significant power in each of the bands during the three phases was tested using the Likelihood ratio test (χ^2(DoF, N)).

Histology

Once the experimental endpoints were met, each animal was deeply anesthetized with sodium pentobarbital and perfused transcardially with perfusion wash (1222SK, 1223SK, super reagent, Electron Microscopy Sciences) followed by 10% formalin perfusion fixative (super reagent, Electron Microscopy Sciences). Fifty micron thick slices were made through the pallidum in the coronal plane to ascertain the location of the DBS lead. Slices were made in the parasagittal plane through the thalamus for the reconstruction of the recording tracks. Alternate slices were stained using acetylcholinesterase (AChE) and cresyl violet. Determination of recording locations to VA/VLo and VPLo was made using both reconstruction of recording locations and the response to microstimulation as described in our previous publications [13,14].

Results

Histological evidence for the location of DBS lead and recording tracks

Fig. 2A shows a sagittal section of the thalamus stained for acetylcholinesterase, with the motor subnuclei of the thalamus as well as other key anatomical structures noted. An example recording track passing through VLo is indicated by the arrowhead. Fig. 2B depicts the trajectory of the DBS lead through the pallidum in the coronal plane stained with cresyl violet.

Behavioral improvement during GPi DBS

The total median mUPDRS scores in the OFF DBS state across the experimental period were 24 (n = 13; IQR: 2) and 15 (n = 20; IQR: 1.25) for monkeys N and S, respectively. Therapeutic GPi DBS significantly improved motor signs in both animals (Fig. 3A). During GPi DBS rigidity and tremor were completely resolved, while significant improvements were achieved in akinesia and bradykinesia (Fisher's exact test: $p < 0.0001$). Although tremor is not a common feature in rhesus monkeys, following MPTP it can occur as a fine postural tremor, and was mildly present in one animal in this study and was abolished during stimulation. The reach time and retrieval time during the Klüver board task were also reduced significantly during DBS for both monkey N (paired t: $t_{15} = -2.4$, $p = 0.032$) and monkey S (paired t: $t_{76} = -4.96$, $p < 0.0001$), with no change in manipulation time for either animal (paired t: N: $t_{15} = -0.27$, $p = 0.8$; S: $t_{76} = -0.2$, $p = 0.8$) (Fig. 3B and C).

Changes in thalamic neuronal activity during GPi DBS

We analyzed spike activity from a total of 134 neurons in VA/VLo and 129 neurons in VPLo after excluding units that did not pass the inclusion criteria explained below. Neuronal activity records were eliminated if they were contaminated with artifacts, did not have activity during all three phases (i.e. pre-, during- and post-DBS), or if there were significant changes in the amplitude and/or shape of the spike waveform across the recording. Additionally, the recording had to be at least 60 s long and the discharge rate was at least 3 Hz in all three phases. Only cells recorded from each sub-nucleus that passed all of the above criteria and were also examined for somatosensory responses to passive manipulation were included in this study. Table 1 summarizes the response characteristics of neurons to passive manipulation and presence or absence of micro-stimulation evoked movement in the region of the recording.

Thalamic response patterns

Neuronal activity in both the pallidal (VA/VLo) and cerebellar (VPLo) receiving areas was altered by GPi DBS, with over half of the cells in each site showing significant suppression during stimulation. A smaller number of units exhibited either tonic excitatory or poly-phasic responses to stimulation, and are depicted in Fig. 1D.

Pallidal receiving area (VA/VLo)

Forty seven percent (n = 62) of neurons in the VA/VLo were inhibited during DBS; 21% (n = 28) were activated; 22% were inhibited-excited (IE; n = 29); 10% were excited-inhibited (EI; n = 13) (Fig. 4A). Of those units that were inhibited, 53.2% were suppressed for the duration of the inter-pulse interval, with the remaining displaying either a biphasic (1.6%) or poly-phasic (45.2%) response pattern. Maximum suppression occurred at a median delay of 4.8 ms (IQR: 2.6) for neurons showing bi- or poly-phasic responses. Of those neurons that increased activity during GPi DBS, tonic, biphasic and poly-phasic responses were observed in 17.9%, 32.1% and 50.0%, respectively. For those units with excitatory bi- or poly-phasic activity, maximum excitation occurred at a median delay of 2.0 ms (IQR: 4.0).

During the post-DBS interval the vast majority of cells demonstrated a prolonged change in activity (n = 113) with 43% of the units exhibiting inhibition of discharge activity with either a tonic (75%) or poly-phasic (25%) pattern. Post DBS there was an increase in the number of units with a predominant excitatory response increasing from 21% in the pre-DBS condition to 4% post-DBS, with 26% having a poly-phasic response and 70% showing persistent activation. All but one of the remaining cells returned to baseline activity levels following cessation of stimulation.

Cerebellar receiving area (VPLo)

A majority of VPLo cells were also inhibited during GPi DBS (48.8%, n = 63), 17% were activated (E, n = 22), while 17% (EI, n = 22) and 13.2% (IE, n = 17) exhibited biphasic responses and 3.1% (n = 4) did not change their activity in response to DBS (Fig. 4B). Forty nine percent of units had a tonic response to DBS, 47.6% had poly-phasic and the rest showed a biphasic response. For the bi-/poly-phasic units the median delay to maximum inhibition was 5.4 ms (IQR: 3.1). Forty five percent of the units that were activated by DBS

discharged tonically, 4.6% bi-phasically and 50% had a poly-phasic response. The median delay in the onset of maximum excitation was 2.2 ms (IQR: 5.0) for the phasic units. In the post-stimulation interval 47% of units were inhibited (tonic: 74%; poly-phasic 26%); however, similar to the VA/VLo, there was an increase in the number of cells with increased activity (17% pre-DBS to 47% post-stimulation); 72% of these units had a poly-phasic response pattern (16%) and the rest exhibited persistent excitation (72%). The remaining cells either exhibited no change relative to the baseline activity (n = 5) or had an IE (n = 1) or EI (n = 1) type of response.

Population mean discharge rate

Although the response type of individual neurons was varied in both thalamic subnuclei, the net effect of GPi DBS was a significant reduction in neuronal spike activity in both VA/VLo (paired t: $t_{134} = 3.1$, $p = 0.0024$) and VPLo ($t_{128} = 3.9$, $p < 0.0001$). The median discharge rates of neurons in VA/VLo pre-, during- and post-DBS were 12 (IQR: 9.5), 10.1 (IQR: 10.3), and 11.9 (IQR: 10.6), respectively. For VPLo the median firing rates of neurons during the three recording intervals were 14.3 (IQR: 9.9), 11.2 (IQR: 8.8), and 13.7 (IQR: 9.2), respectively. For neurons demonstrating a tonic inhibitory response to GPi DBS, the median reductions in discharge rate were 34.2 ± 26.5% and 31.4 ± 19.8% for the VA/VLo and VPLo, respectively (Fig. 5). The change in discharge rate during DBS relative to the pre-DBS state was not significantly different between the two nuclei, either when all of the neurons were pooled (Wilcoxon rank sum: $Z = -0.76$, $p = 0.45$) or when only those classified as inhibited by DBS were considered ($Z = -0.89$, $p = 0.37$). Following discontinuation of stimulation, although the per cent of cells with a predominant inhibitory pattern tended to persist following DBS, the overall population mean discharge rate of cells in both the VA/VLo (paired t: $t_{134} = 0.68$, $p = 0.5$) and the VPLo reverted towards baseline activity levels ($t_{128} = 0.16$, $p = 0.87$), likely a result of the increased number of cells with an excitatory pattern in the post-DBS period.

Bursting activity

GPi DBS changed the structure of bursts in both subnuclei (Fig. 6), resulting in longer bursts, with lower and more variable inter-spike intervals. Median and inter-quartile range for measures of bursting activity in the pre-, during- and post-DBS intervals are summarized in Table 2. Almost all of the VA/VLo (n = 132/134) and VPLo (n = 128/129) neurons analyzed in this study had at least one burst discharge during the recording window. As we did not arbitrarily set a minimum criterion in terms of percent time with bursts or number of bursts, the percent of cells with bursts during the baseline interval for each sub-nucleus is high.

GPi DBS affected several measures of bursting activity in the VA/VLo (Fig. 6A–C left column) decreasing the intra-burst rate (IBR; paired t: $t_{131} = 3.3$, $p = 0.0011$), while increasing burst duration ($t_{131} = -5.2$, $p < 0.0001$), median-burst ISI ($t_{131} = -6.6$, $p < 0.0001$) and the variability in the ISI ($t_{131} = -9.6$, $p < 0.0001$). Although there was a tendency for burst frequency and percent spikes within bursts to increase during GPi DBS, the difference did not reach significance after correcting for multiple comparisons. The change in mean IBR ($t_{131} = 5$, $p < 0.0001$), burst duration ($t_{131} = -5.3$, $p < 0.0001$), median-

burst ISI ($t_{131} = -5.5$, $p < 0.0001$) and variability in the ISI ($t_{131} = -8.6$, $p < 0.0001$) persisted following cessation of stimulation.

In VPLo (Fig. 6A–C right column), GPi DBS significantly reduced the intra-burst rate (paired t: $t_{127} = 4.7$, $p < 0.0001$). Percent spikes within bursts ($t_{127} = -4.9$, $p < 0.0001$), burst frequency ($t_{127} = -4.5$, $p < 0.0001$), burst duration ($t_{127} = -3.9$, $p < 0.0001$), median-burst ISI ($t_{127} = -7.1$, $p < 0.0001$) and the variability of the burst ISIs ($t_{127} = -6.8$, $p < 0.0001$) increased during DBS. In the post-DBS interval, IBR ($t_{127} = 4.4$, $p < 0.0001$) remained reduced, and burst duration ($t_{127} = -3.3$, $p = 0.0014$), median ISI ($t_{127} = -5.6$, $p < 0.0001$) and variability in the ISI ($t_{127} = -6.6$, $p < 0.0001$) remained elevated relative to the pre-DBS interval. Although the burst frequency and percent of spikes within bursts were higher in the post- than the pre-DBS state, the difference did not reach significance.

Comparison of burst structures using the rank-sum test, between units that were inhibited or excited during DBS, revealed differences in IBR ($z_{127} = -2.2$; $p = 0.03$), burst duration ($z_{131} = 2.6$; $p = 0.0095$) and burst frequency ($z_{131} = 2.2$; $p = 0.03$) in the VA/VLo. In VPLo, IBR (rank sum; $z_{127} = -3.4$; $p < 0.0001$), burst duration ($z_{127} = 3.3$; $p < 0.0001$) and median ISI ($z_{127} = 3.0$; $p = 0.0026$) were significantly different in the post DBS interval. Recording times were not long enough to determine the relative time required for cells to return to baseline activity and this is a limitation of the present study. It is unlikely that the post DBS persistent changes in rate and pattern are due to a natural change in the rate and pattern given how consistent these changes were across neurons. Cell rates and patterns can change to varying degrees when recording over long periods, however the consistent and persistent changes we observed post DBS together with the small number of cells that were recorded for longer periods of time that did show a return to pre DBS levels suggest it was a persistent effect of DBS.

In the post-stimulation phase, units that were inhibited during DBS continued to have higher IBR (VA/VLo: $z = 2.2$, $p = 0.03$; VPLo: $z = 3.3$, $p < 0.0001$), and lower burst duration (VA/VLo: $z = -2.6$, $p = 0.01$; VPLo: $z = -3.3$, $p < 0.0001$) relative to the cells that were excited by DBS. Median ISI (VA/VLo: not significant; VPLo: $z = -2.9$, $p = 0.004$) and burst frequency (VA/VLo: $z = -2.2$, $p = 0.03$; VPLo: not significant) were not significantly changed in the post-stimulation phase. These data suggest that the sustained inhibition during DBS was associated with particular changes in burst structure that generally persisted in the post DBS period in both VA/VLo and VPLo.

Oscillatory activity

Example of power spectra, percent of cells with significant power in the seven frequency bands within the 0–150 Hz range and the distribution of peak frequencies within the 90–150 Hz band are shown for VA/VLo and VPLo in Fig. 7A and B, respectively. The number of cells with significant oscillatory activity in the 90–150 Hz band was increased during DBS relative to baseline activity, both in the VA/VLo (likelihood ratio: $\chi^2(1268) = 22.8$, $p < 0.0001$) and VPLo ($\chi^2(1258) = 15.0$, $p < 0.0001$) (Fig. 7A and B ii). The distribution of peak frequencies within the same band was also significantly different between the pre-DBS and DBS intervals in both the VA/VLo (Kolmogorov–Smirnov: $D_{43,\,82} = 0.30$, $p < 0.0001$; Fig. 7A iii) and VPLo ($D_{43,\,74} = 0.27$, $p < 0.0001$; Fig. 7B iii); the median oscillatory

frequency during the pre-DBS interval was 120.4 (IQR: 31.6) and 117.2 (IQR: 32.2) for neurons in VA/VLo and VPLo, respectively. During DBS the peak frequency shifted to 136.2 Hz (IQR: 22.7) in both subnuclei. Forty-four units in VA/VLo had peak frequency in the 130–140 Hz range; 40.9%, 6.8%, 38.7% and 13.6% of these neurons were classified as inhibited, excited, inhibited-excited or excited-inhibited during DBS, respectively; in the VPLo also 44 units had peak frequency in 130–140 Hz range, and the proportions of these units inhibited, excited, inhibited-excited, excited-inhibited or not affected by DBS were: 47.7%, 9.1%, 36.4%, 4.6% and 2.3%. Although peaks in the theta, alpha, low beta and high beta bands were present in the spectra of a few cells, we did not observe a change in these peaks during GPi DBS in either thalamic sub-nucleus.

Discussion

In this study, we examined neuronal activity changes in the motor thalamus during therapeutic GPi stimulation in two moderately parkinsonian monkeys, relative to the pre-DBS control state; sub-therapeutic stimulation as a secondary control state was not evaluated in this study (see study limitations section). Stimulation of GPi produced a variety of activity changes across both the pallidal and cerebellar receiving areas of the motor thalamus, including DBS-induced reductions in mean discharge rate, changes in burst characteristics as well as shifts in oscillatory behavior marked by an increase in high frequency spectral activity across both thalamic subnuclei. The predominant effect of GPi DBS was suppression of neuronal activity in the pallidal receiving area (VA/VLo), as revealed by both an overall change in the population discharge rate as well as by the proportionally high incidence of individual neurons showing a tonic inhibition pattern. This observation is consistent with our hypothesis that high-frequency DBS activates inhibitory GABAergic projections from GPi to VA/VLo [3,20]. An unanticipated finding was that the predominant effect of GPi DBS on the cerebellar receiving area of the motor thalamus (VPLo) was also inhibition; despite the absence, insofar as is currently known, of direct projections from the GPi to the VPLo. One possible mechanism for this observation may relate to a secondary reduction in cholinergic excitatory inputs from the pedunculopontine tegmental nucleus [21] or other brainstem, cerebellar or spinal areas [22,23] due to chronic activation of GPi GABAergic output to these regions [24]. Interestingly, a small subset of neurons within each subnucleus increased their mean discharge rate during DBS, likely as a further reflection of the multiple pathways impacted by GPi DBS whose delays in effect likely produce the poly-phasic responses observed in both subnuclei.

Patterns of response

Inspection of the PSTH, triggered on the stimulation pulses, revealed four distinct response patterns of VA/VLo neurons during high frequency stimulation of GPi; 47% of motor thalamic neurons showed a reduction in discharge frequency, 21% increased, and the rest showed a mixed pattern of inhibition followed by excitation, or excitation followed by inhibition. Previous studies examining the effect of GPi DBS on pallidal activity have reported opposing effects, with one study reporting that a majority of the neurons were activated by GPi DBS [16], while another reported a significant decrease in the firing rate of pallidal neurons in the region of stimulation [25]. Others, however, have reported complex

neuronal responses at the site of stimulation, with some cells activated while others were suppressed [4,26,27], similar to that reported during STN DBS [9]. These differential effects of STN/GPi DBS on thalamic activity are further supported by micro-dialysis studies examining the change in neurotransmitter levels in the thalamus during DBS. Stefani et al. have reported reduced levels of GABA in the VA, during STN DBS [28], suggesting a reduction in GPi output to the VA and could potentially correlate with the subset of units that were excited during DBS in this study. This finding would suggest that DBS suppresses output from the stimulated structure. Multiple other studies, however, have reported increased cGMP levels in the GPi [28] [29] [30] and in the SNr [30] during STN DBS suggesting increased levels of synaptic/metabolic activity consistent with activation of output from the stimulated structure. Regardless of whether one supports the inhibition or activation hypothesis, the far-reaching effect of DBS on other structures in the circuit is supported by a number of studies demonstrating alterations in cortical activity with STN [31] [32] or GPi DBS [33] as well as previous modeling [34,35] and animal studies recording from multiple structures in the circuit [9,24] [36–38]. Changes in extracellular concentrations of striatal GABA and glutamate during STN stimulation lend further support to the varied and complex changes that occur during DBS [39,40].

The variety of response patterns of VA/VLo neurons observed in this study may likely reflect not only the complex patterns that occur in the pallidum during DBS, but also the differential effects of stimulation on neurons and fibers of passage at varying distances from the site of stimulation. In support of this hypothesis is our observation that a majority (55%) of the VPLo neurons that were excited by GPi DBS had bi-phasic or poly-phasic discharge patterns, which suggests that multiple and/or multi-synaptic pathways are likely involved in mediating these responses [41]. Given we did not vary stimulation frequency or patterns the latency of the change in thalamic activity relative to the stimulation pulse in GPi does not allow one to discern which pathways are directly responsible for the observed changes or to what degree, nor was it the intent of this study to make such a determination. It is likely, however, that the early inhibitory effect on VA/VPLo is due to the direct inhibitory projection from GPi to VA/VLo. It is much more difficult to understand the inhibitory effect on VPLo; however there are multiple potential pathways that could contribute including the effect of GPi projections to the PPN which in turn project to both VA/VLo and VPLo as well as the reticular nucleus of the thalamus. Excitatory changes could arise from activation of premotor, supplementary motor or primary motor cortical projections to the motor thalamus or indirectly through projections from the cerebellum. Understanding which pathways are responsible for the observed changes and to what degree becomes even more complex when one takes into account the dissociation between the effect of stimulation on the cell soma versus that which occurs at the level of the axon [42].

Comparison to STN DBS

The effect of GPi DBS on VA/VLo neuronal activity was similar to that reported during STN DBS [7] and can be explained by the fact that both STN and GPi DBS activate GPi output. The difference however is in the relative effect of stimulation in these sites on VPLo neuronal activity: STN activates a majority of VPLo neurons, while GPi stimulation inhibits a majority of them. This difference is likely due to the fact that DBS in the area of the STN

activates cerebellothalamic projections that lie in close physical proximity to the posterodorsal portion of the STN. The clinical significance of this finding may lie in the relative temporal effect of STN to GPi DBS on tremor suppression with STN providing a more immediate effect similar to that seen with Vim DBS, while GPi DBS generally takes longer to elicit its full effect on tremor suppression. We hypothesize that the delay in tremor suppression during GPi DBS could be due, at least in part, to the inhibitory effect of GPi DBS on VPLo neurons together with the multi-synaptic pathway(s) mediating this effect and observed poly-phasic response pattern.

Helmich et al. [43] have put forward the “Dimmer-Switch” hypothesis to explain the role of the GPi in tremorgenesis; as per this hypothesis, 8–20 Hz oscillations in GPi discharge trigger tremor frequency bursts in the pallidal thalamus, which then enters the tremor generating cerebello-thalamo-cortical circuit through the motor cortical areas. In this model it is the cerebello-thalamo-cortical network that is the ultimate tremor generator, but as influenced and triggered by the coupled basal ganglia network. Since both STN and GPi DBS affect activity in both the pallido and cerebellar thalamic circuits one can explain their beneficial effect on tremor. There is, however, a difference between the times of stimulation onset to improvement in tremor between these sites with STN DBS having a more immediate effect on tremor. The opposing effects of STN and GPi DBS on VPLo activity, STN stimulation activates VPLo neurons, while GPi DBS suppresses them, could explain this difference together with the fact that STN DBS has an immediate and direct effect on motor cortical activity via antidromic activation of the hyper-direct pathway [32]. Thus, STN DBS could alleviate PD tremor by activation of corticothalamic and cerebellothalamic pathways [32,44], a mechanism that could be similar to the suppression of PD tremor observed during voluntary movement.

Bursting activity

In addition to a significant reduction in mean discharge rate, GPi DBS also had a significant effect on bursting activity in the motor thalamus. There was a change in the structure of bursts during GPi DBS in both subnuclei and although we did not observe a reduction in the number of bursts/minute, we did find a change in the structure or individual bursts. This result is in agreement with previously published data on the effects of therapeutic GPi DBS on neurons in the GPi and thalamus, respectively [3,27]. In both studies, the authors reported a reduction in bursting activity, entrainment of cells and complex responses in the interval between DBS pulses. Computational modeling of information transfer through the basal-ganglia-thalamic network previously suggested that therapeutic DBS regularized basal ganglia activity, thereby minimizing transmission errors by the thalamus, and was associated with motor symptom alleviation [45,46]. This suggests that changes to the pathological bursting activity in the thalamus during GPi DBS would be associated with improved transfer of information via the motor thalamus to the cortex and other sites that receive projections from the thalamus and may be one of the mechanisms through which DBS improves PD symptoms [27,47].

Persistence of the effects of DBS

Another significant finding of this study is the persistence of DBS induced changes in bursting activity and neuronal discharge patterns in the post-stimulation interval. It has been demonstrated that motor signs improve and return with some delay during and immediately following DBS. The persistent change in neuronal activity observed in this study following cessation of stimulation could explain the residual therapeutic effects seen when DBS is turned off [1]. The persistence of the therapeutic benefits for several minutes post-stimulation suggests that, if a reliable biomarker for the return of the symptoms could be identified, then continuous DBS could be replaced with a closed-loop stimulation system based on the appropriate biomarker [48,49]. Alternatively, stimulation patterns that could potentiate this plastic effect on neuronal activity, similar to that proposed by Tass et al. [50], could be used either alone or in conjunction with a closed-loop system that could markedly prolong battery life for current devices and potentiate improvement of motor signs during the closed-loop phase of stimulation.

Oscillatory activity

Dynamic changes in oscillatory activity across the basal ganglia thalamo-cortical network likely have a key functional role in motor behavior and multiple hypotheses have arisen regarding the role of such oscillatory activity in both normal and abnormal brain functions [51,52]. Specifically, oscillations in the 11–20 Hz range (the low beta band) in particular have been implicated in PD pathophysiology [53,54]. Further support for the role of beta activity in the pathogenesis of PD motor signs is the report that stimulation at beta frequencies worsened parkinsonian symptoms [55,56]. Other studies have suggested that the impairment in the amplitude and timing of modulation of beta activity, relative to specific movement epochs, might underlie bradykinesia and rigidity [57,58]. While still others debate on the role of beta activity in PD noting that it is not present in all patients [59] or may be related to cueing of movement [58]. Indeed our own observation is that beta activity is present in the normal condition in nonhuman primates and does not correlate with increasing severity of the parkinsonian state [60]. While not excluding it as a biomarker for adaptive stimulation, see Little et al. [49], it also suggests that the mere increase in the occurrence of beta band activity is not pathognomonic of the parkinsonian state. We believe that the extent of impairment of the timing and depth of modulation of beta activity is likely to be a better predictor of disease severity [61].

The main change in oscillatory activity seen in this study was an increase in power of high frequency oscillatory activity in the gamma range likely due to the entrainment of a subset of cells to the stimulation pulse, which occurred in both subnuclei. We did not observe a significant reduction in beta activity in the thalamus during stimulation contrary to that which has been reported in the STN and GPi during DBS [16,62]. In fact, very few cells in the VA/VLo and VPLo had peaks in tremor and beta frequency bands. The observed increase in higher frequency oscillatory activity is consistent with a regularization of neuronal activity and entrainment of a large number of neurons in the motor thalamus to the stimulation pulse. In addition, one cannot exclude the potential role of the reduction in bursting activity reported by others as well as the change in burst characteristics observed in this study. These factors also likely to contribute to the therapeutic effects of DBS and agree

with computational models exploring the role of irregular bursting patterns of activity on information processing [27,46,47].

Study limitations

The data presented in this study were collected using clinically relevant stimulation parameters and with macro-electrodes scaled down to replicate the human DBS leads. However, we did not assess the effects of DBS at sub-therapeutic amplitude(s) or at a lower frequency. That being said, Xu et al. compared the effect of STN DBS on VA/VLo and VPLo neurons to both sub-therapeutic and OFF stimulation conditions; they reported that there was no significant difference in the activity of the neurons between the DBS OFF and sub-therapeutic stimulation condition [7]. Hence, we believe that the lack of sub-therapeutic control does not invalidate the results reported here. Stimulation at a lower frequency would have allowed a more detailed assessment of the time course of changes in the thalamus from the DBS pulse and not just the pooled response over a minute. As such we were unable to determine why both VA/VLo and VPLo neurons exhibited responses with similar latencies despite the lack of currently known direct pathways from the GPi to the cerebellar thalamic nucleus. The lack of this information also makes it hard to determine the contributions of pathways that either pass through or are in the vicinity of the GPi, to the poly-phasic responses seen in the PSTH of neurons recorded from both the VA/VLo and VPLo. Stimulation at one or more sub-therapeutic amplitudes would have allowed us to determine the contributions of different nuclei and fiber pathways to the net effect of DBS on PD symptoms. The short duration of the recording in the post-stimulation interval precludes our ability to assess the persistence of therapeutic effects of DBS and to correlate the changes in the neuronal activity with the return of PD symptoms. Another shortcoming of this study was the small sample of simultaneous recordings from multiple units to assess synchronization within and between nuclei. Attempts will be made in future studies to record from multiple nuclei simultaneously over longer time periods that will position us to better substantiate hypotheses regarding network level mechanisms of therapeutic DBS. Lastly, the presence of peaks at the stimulation frequency could point some to consider the regularization of activity as artifactual. However, given that the same artifact removal method was applied to all units, and only 30% of units with a variety of response types (i.e., inhibition, excitation etc.) had a peak at/near the DBS frequency, is compelling evidence to support the biological basis for this observation.

Conclusion

In summary, understanding how DBS works is more complex than changing any one physiological parameter. Multiple mechanisms are in play, producing differential effects on upstream as well as downstream neurons throughout the basal ganglia thalamo-cortical network. In the current study GPi DBS produced a number of changes in thalamic neuronal activity, including (1) shifting the power spectra of the neuronal oscillatory activity from lower to higher (gamma) frequency ranges, (2) changing the structure of bursting activity, (3) altering in the discharge rate and (4) regularizing the activity of thalamic neurons. Many questions remain, we still do not understand how these changes affect the ability of the network to transfer and process information, to respond to perturbations in the system or

how commands initiated elsewhere in the brain may be affected by these changes. These questions remain unanswered but will need to be addressed if we are to optimize our ability to use this tool in the treatment of not only PD but to be able to expand its therapeutic effect to other neurological and psychiatric disorders.

Acknowledgements

This study was supported by NIH R01 NS-037019 and a postdoctoral fellowship for basic scientists awarded to the author by Parkinson's Disease Foundation PDF-FBS-1105. We would like to thank Medtronic for providing us with the pulse generator (Itrel II) used in this study. We would like to thank Dr. Claudia Hendrix for helping with statistical analysis of data.

References

1. Temperli P, Ghika J, Villemure JG, Burkhard PR, Bogousslavsky J, Vingerhoets FJ. How do parkinsonian signs return after discontinuation of subthalamic DBS? Neurology. 2003; 60:78–81. [PubMed: 12525722]
2. Vitek JL. Deep brain stimulation for Parkinson's disease. A critical re-evaluation of STN versus GPi DBS. Stereotact Funct Neurosurg. 2002; 78:119–31. [PubMed: 12652037]
3. Anderson ME, Postupna N, Ruffo M. Effects of high-frequency stimulation in the internal globus pallidus on the activity of thalamic neurons in the awake monkey. J Neurophysiol. 2003; 89:1150–60. [PubMed: 12574488]
4. Montgomery EB Jr. Effects of GPi stimulation on human thalamic neuronal activity. Clin Neurophysiol. 2006; 117:2691–702. [PubMed: 17029953]
5. Pralong E, Debatisse D, Maeder M, Vingerhoets F, Ghika J, Villemure JG. Effect of deep brain stimulation of GPI on neuronal activity of the thalamic nucleus ventralis oralis in a dystonic patient. Neurophysiol Clin. 2003; 33:169–73. [PubMed: 14519544]
6. Elder, CM.; Vitek, JL. The motor thalamus: alteration of neuronal activity in the parkinsonian state.. In: Kultas-Ilinsky, K.; Ilinsky, IA., editors. Basal ganglia and thalamus in health and movement disorders. Springer; 2001. p. 257-65.
7. Xu W, Russo GS, Hashimoto T, Zhang J, Vitek JL. Subthalamic nucleus stimulation modulates thalamic neuronal activity. J Neurosci. 2008; 28:11916–24. [PubMed: 19005057]
8. Miocinovic S, Noecker AM, Maks CB, Butson CR, McIntyre CC. Cicerone: stereotactic neurophysiological recording and deep brain stimulation electrode placement software system. Acta Neurochir Suppl. 2007; 97:561–7. [PubMed: 17691348]
9. Hashimoto T, Elder CM, Okun MS, Patrick SK, Vitek JL. Stimulation of the subthalamic nucleus changes the firing pattern of pallidal neurons. J Neurosci. 2003; 23:1916–23. [PubMed: 12629196]
10. Fahn, S.; Marsden, CD.; Jenner, P. Unified Parkinson's disease rating scale.. In: Teychenne, P., editor. Recent developments in Parkinson's disease. Raven Press; San Diego: 1986. p. 153-64.
11. Vitek JL, Bakay RA, Hashimoto T, Kaneoke Y, Mewes K, Zhang JY, et al. Microelectrode-guided pallidotomy: technical approach and its application in medically intractable Parkinson's disease. J Neurosurg. 1998; 88:1027–43. [PubMed: 9609298]
12. Elder CM, Hashimoto T, Zhang J, Vitek JL. Chronic implantation of deep brain stimulation leads in animal models of neurological disorders. J Neurosci Methods. 2005; 142:11–16. [PubMed: 15652612]
13. Vitek JL, Ashe J, DeLong MR, Kaneoke Y. Microstimulation of primate motor thalamus: somatotopic organization and differential distribution of evoked motor responses among subnuclei. J Neurophysiol. 1996; 75:2486–95. [PubMed: 8793758]
14. Vitek JL, Ashe J, DeLong MR, Alexander GE. Physiologic properties and somatotopic organization of the primate motor thalamus. J Neurophysiol. 1994; 71:1498–513. [PubMed: 8035231]

15. Hashimoto T, Elder CM, Vitek JL. A template subtraction method for stimulus artifact removal in high-frequency deep brain stimulation. J Neurosci Methods. 2002; 113:181–6. [PubMed: 11772439]
16. McCairn KW, Turner RS. Deep brain stimulation of the globus pallidus internus in the parkinsonian primate: local entrainment and suppression of low-frequency oscillations. J Neurophysiol. 2009; 101:1941–60. [PubMed: 19164104]
17. Legendy CR, Salcman M. Bursts and recurrences of bursts in the spike trains of spontaneously active striate cortex neurons. J Neurophysiol. 1985; 53:926–39. [PubMed: 3998798]
18. Bokil H, Andrews P, Kulkarni JE, Mehta S, Mitra PP. Chronux: a platform for analyzing neural signals. J Neurosci Methods. 2010; 192:146–51. [PubMed: 20637804]
19. Rivlin-Etzion M, Ritov Y, Heimer G, Bergman H, Bar-Gad I. Local shuffling of spike trains boosts the accuracy of spike train spectral analysis. J Neurophysiol. 2006; 95:3245–56. [PubMed: 16407432]
20. Vitek JL. Mechanisms of deep brain stimulation: excitation or inhibition. Mov Disord. 2002; 17(Suppl. 3):S69–72. [PubMed: 11948757]
21. Garcia-Rill E. The pedunculopontine nucleus. Prog Neurobiol. 1991; 36:363–89. [PubMed: 1887068]
22. Jackson A, Crossman AR. Nucleus tegmenti pedunculopontinus: efferent connections with special reference to the basal ganglia, studied in the rat by anterograde and retrograde transport of horseradish peroxidase. Neuroscience. 1983; 10:725–65. [PubMed: 6646427]
23. Sofroniew MV, Priestley JV, Consolazione A, Eckenstein F, Cuello AC. Cholinergic projections from the midbrain and pons to the thalamus in the rat, identified by combined retrograde tracing and choline acetyltransferase immunohistochemistry. Brain Res. 1985; 329:213–23. [PubMed: 3978443]
24. Zhang J, Wang ZI, Baker KB, Vitek JL. Effect of globus pallidus internus stimulation on neuronal activity in the pedunculopontine tegmental nucleus in the primate model of Parkinson's disease. Exp Neurol. 2012; 233:575–80. [PubMed: 21821025]
25. Boraud T, Bezard E, Bioulac B, Gross C. High frequency stimulation of the internal Globus Pallidus (GPi) simultaneously improves parkinsonian symptoms and reduces the firing frequency of GPi neurons in the MPTP-treated monkey. Neurosci Lett. 1996; 215:17–20. [PubMed: 8880743]
26. Bar-Gad I, Elias S, Vaadia E, Bergman H. Complex locking rather than complete cessation of neuronal activity in the globus pallidus of a 1-methyl-4-phenyl-1,2,3,6-tetrahydropyridine-treated primate in response to pallidal microstimulation. J Neurosci. 2004; 24:7410–19. [PubMed: 15317866]
27. Cleary DR, Raslan AM, Rubin JE, Bahgat D, Viswanathan A, Heinricher MM, et al. Deep brain stimulation entrains local neuronal firing in human globus pallidus internus. J Neurophysiol. 2013; 109:978–87. [PubMed: 23197451]
28. Stefani A, Fedele E, Pierantozzi M, Galati S, Marzetti F, Peppe A, et al. Reduced GABA content in the motor thalamus during effective deep brain stimulation of the subthalamic nucleus. Front Syst Neurosci. 2011; 5:17. [PubMed: 21519387]
29. Stefani A, Fedele E, Vitek J, Pierantozzi M, Galati S, Marzetti F, et al. The clinical efficacy of L-DOPA and STN-DBS share a common marker: reduced GABA content in the motor thalamus. Cell Death Dis. 2011; 2:e154. [PubMed: 21544093]
30. Windels F, Bruet N, Poupard A, Urbain N, Chouvet G, Feuerstein C, et al. Effects of high frequency stimulation of subthalamic nucleus on extracellular glutamate and GABA in substantia nigra and globus pallidus in the normal rat. Eur J Neurosci. 2000; 12:4141–6. [PubMed: 11069610]
31. de Hemptinne C, Swann NC, Ostrem JL, Ryapolova-Webb ES, San Luciano M, Galifianakis NB, et al. Therapeutic deep brain stimulation reduces cortical phase-amplitude coupling in Parkinson's disease. Nat Neurosci. 2015; 18:779–86. [PubMed: 25867121]
32. Li Q, Ke Y, Chan DC, Qian ZM, Yung KK, Ko H, et al. Therapeutic deep brain stimulation in parkinsonian rats directly influences motor cortex. Neuron. 2012; 76:1030–41. [PubMed: 23217750]

33. McCairn KW, Turner RS. Pallidal stimulation suppresses pathological dysrhythmia in the parkinsonian motor cortex. J Neurophysiol. 2015; 113:2537–48. [PubMed: 25652922]
34. McIntyre CC, Mori S, Sherman DL, Thakor NV, Vitek JL. Electric field and stimulating influence generated by deep brain stimulation of the subthalamic nucleus. Clin Neurophysiol. 2004; 115:589–95. [PubMed: 15036055]
35. McIntyre CC, Savasta M, Kerkerian-Le Goff L, Vitek JL. Uncovering the mechanism(s) of action of deep brain stimulation: activation, inhibition, or both. Clin Neurophysiol. 2004; 115:1239–48. [PubMed: 15134690]
36. Zimnik AJ, Nora GJ, Desmurget M, Turner RS. Movement-related discharge in the macaque globus pallidus during high-frequency stimulation of the subthalamic nucleus. J Neurosci. 2015; 35:3978–89. [PubMed: 25740526]
37. Agnesi F, Connolly AT, Baker KB, Vitek JL, Johnson MD. Deep brain stimulation imposes complex informational lesions. PLoS ONE. 2013; 8:e74462. [PubMed: 23991221]
38. Anderson CJ, Sheppard DT, Huynh R, Anderson DN, Polar CA, Dorval AD. Subthalamic deep brain stimulation reduces pathological information transmission to the thalamus in a rat model of parkinsonism. Front Neural Circuits. 2015; 9:31. [PubMed: 26217192]
39. Bruet N, Windels F, Carcenac C, Feuerstein C, Bertrand A, Poupard A, et al. Neurochemical mechanisms induced by high frequency stimulation of the subthalamic nucleus: increase of extracellular striatal glutamate and GABA in normal and hemiparkinsonian rats. J Neuropathol Exp Neurol. 2003; 62:1228–40. [PubMed: 14692699]
40. Windels F, Bruet N, Poupard A, Feuerstein C, Bertrand A, Savasta M. Influence of the frequency parameter on extracellular glutamate and gamma-aminobutyric acid in substantia nigra and globus pallidus during electrical stimulation of subthalamic nucleus in rats. J Neurosci Res. 2003; 72:259–67. [PubMed: 12672001]
41. Johnson MD, Zhang J, Ghosh D, McIntyre CC, Vitek JL. Neural targets for relieving parkinsonian rigidity and bradykinesia with pallidal deep brain stimulation. J Neurophysiol. 2012; 108:567–77. [PubMed: 22514292]
42. McIntyre CC, Grill WM, Sherman DL, Thakor NV. Cellular effects of deep brain stimulation: model-based analysis of activation and inhibition. J Neurophysiol. 2004; 91:1457–69. [PubMed: 14668299]
43. Helmich RC, Hallett M, Deuschl G, Toni I, Bloem BR. Cerebral causes and consequences of parkinsonian resting tremor: a tale of two circuits? Brain. 2012; 135:3206–26. [PubMed: 22382359]
44. Stover NP, Okun MS, Evatt ML, Raju DV, Bakay RA, Vitek JL. Stimulation of the subthalamic nucleus in a patient with Parkinson disease and essential tremor. Arch Neurol. 2005; 62:141–3. [PubMed: 15642861]
45. Dorval AD, Kuncel AM, Birdno MJ, Turner DA, Grill WM. Deep brain stimulation alleviates parkinsonian bradykinesia by regularizing pallidal activity. J Neurophysiol. 2010; 104:911–21. [PubMed: 20505125]
46. Guo Y, Rubin JE, McIntyre CC, Vitek JL, Terman D. Thalamocortical relay fidelity varies across subthalamic nucleus deep brain stimulation protocols in a data-driven computational model. J Neurophysiol. 2008; 99:1477–92. [PubMed: 18171706]
47. Agarwal R, Sarma SV. The effects of DBS patterns on basal ganglia activity and thalamic relay : a computational study. J Comput Neurosci. 2012; 33:151–67. [PubMed: 22237601]
48. Rosin B, Slovik M, Mitelman R, Rivlin-Etzion M, Haber SN, Israel Z, et al. Closed-loop deep brain stimulation is superior in ameliorating parkinsonism. Neuron. 2011; 72:370–84. [PubMed: 22017994]
49. Little S, Pogosyan A, Neal S, Zavala B, Zrinzo L, Hariz M, et al. Adaptive deep brain stimulation in advanced Parkinson disease. Ann Neurol. 2013; 74(3):449–57. [PubMed: 23852650]
50. Tass PA, Qin L, Hauptmann C, Dovero S, Bezard E, Boraud T, et al. Coordinated reset has sustained aftereffects in parkinsonian monkeys. Ann Neurol. 2012; 72:816–20. [PubMed: 23280797]
51. Jenkinson N, Brown P. New insights into the relationship between dopamine, beta oscillations and motor function. Trends Neurosci. 2011; 34:611–18. [PubMed: 22018805]

52. Little S, Brown P. The functional role of beta oscillations in Parkinson's disease. Parkinsonism Relat Disord. 2014; 20(Suppl. 1):S44–8. [PubMed: 24262186]

53. Marsden JF, Limousin-Dowsey P, Ashby P, Pollak P, Brown P. Subthalamic nucleus, sensorimotor cortex and muscle interrelationships in Parkinson's disease. Brain. 2001; 124:378–88. [PubMed: 11157565]

54. Brown P, Oliviero A, Mazzone P, Insola A, Tonali P, Di Lazzaro V. Dopamine dependency of oscillations between subthalamic nucleus and pallidum in Parkinson's disease. J Neurosci. 2001; 21:1033–8. [PubMed: 11157088]

55. Eusebio A, Chen CC, Lu CS, Lee ST, Tsai CH, Limousin P, et al. Effects of low-frequency stimulation of the subthalamic nucleus on movement in Parkinson's disease. Exp Neurol. 2008; 209:125–30. [PubMed: 17950279]

56. Gradinaru V, Mogri M, Thompson KR, Henderson JM, Deisseroth K. Optical deconstruction of parkinsonian neural circuitry. Science. 2009; 324:354–9. [PubMed: 19299587]

57. Doyle LM, Kuhn AA, Hariz M, Kupsch A, Schneider GH, Brown P. Levodopa-induced modulation of subthalamic beta oscillations during self-paced movements in patients with Parkinson's disease. Eur J Neurosci. 2005; 21:1403–12. [PubMed: 15813950]

58. Leventhal DK, Gage GJ, Schmidt R, Pettibone JR, Case AC, Berke JD. Basal ganglia beta oscillations accompany cue utilization. Neuron. 2012; 73:523–36. [PubMed: 22325204]

59. Rosa M, Giannicola G, Servello D, Marceglia S, Pacchetti C, Porta M, et al. Subthalamic local field beta oscillations during ongoing deep brain stimulation in Parkinson's disease in hyperacute and chronic phases. Neurosignals. 2011; 19:151–62. [PubMed: 21757872]

60. Connolly AT, Jensen AL, Bello EM, Netoff TI, Baker KB, Johnson MD, et al. Modulations in oscillatory frequency and coupling in globus pallidus with increasing parkinsonian severity. J Neurosci. 2015; 35:6231–40. [PubMed: 25878293]

61. Johnson LA, Nebeck SD, Muralidharan A, Johnson MD, Baker KB, Vitek JL. Closed-loop deep brain stimulation effects on parkinsonian motor symptoms in a non-human primate—Is beta enough? Brain Stimul. 2016 doi:10.1016/ j.brs.2016.06.051.

62. Kuhn AA, Kupsch A, Schneider GH, Brown P. Reduction in subthalamic 8–35 Hz oscillatory activity correlates with clinical improvement in Parkinson's disease. Eur J Neurosci. 2006; 23:1956–60. [PubMed: 16623853]

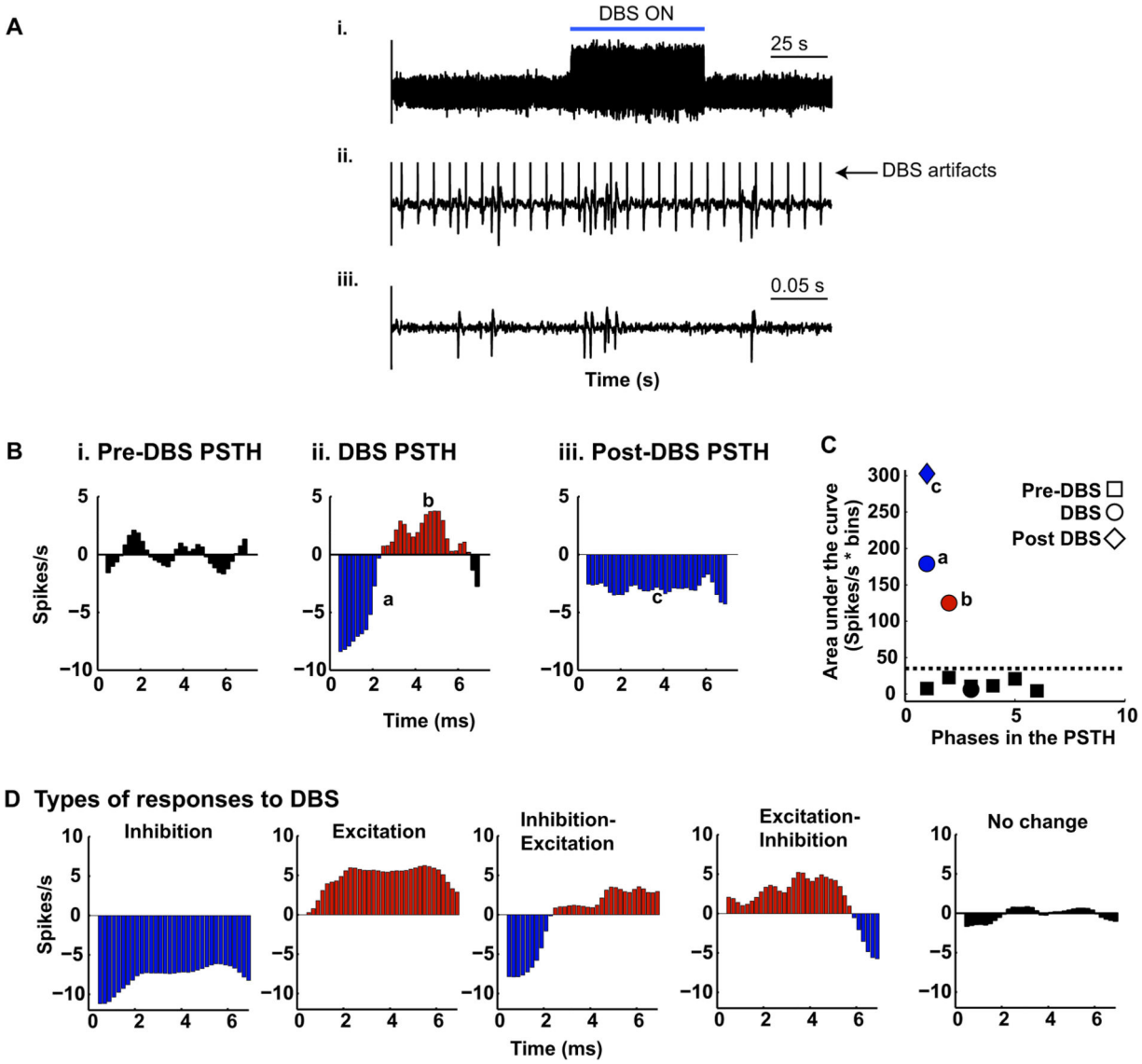

Figure 1.

DBS artifact removal and quantifying the peri stimulus time histogram. (A) Representative example plot showing effective DBS artifact removal using template subtraction. (B) Explanation of the method used to quantify the peri stimulus time histogram for the pre-DBS (i), DBS (ii), and post stimulation (iii) intervals. Pseudo pulses at 135 Hz were used to generate the PSTHs for the pre and post DBS intervals. The mean of the pre-DBS PSTH was subtracted from the during- and post-DBS PSTHs (zero line in B ii and iii). The area enclosed by the PSTH curve and the zero line was computed for the pre-, during and post-DBS intervals (black, blue and red shaded regions in i–iii). (C) Area enclosed by the PSTH curve and the zero crossing line (black, blue and red shaded regions in B i–iii). Three standard deviations above the mean area under the curve(s) for the pre-stimulation interval were set as the threshold (black dotted line). In this example, although the PSTH during DBS has multiple phases, only two of them are greater than the threshold (marked ‘a’ and ‘b’ in B and C); hence, this cell will be designated as having an “inhibited-excited” response

to DBS. The post-stimulation PSTH has one significant phase marked with the small letter ‘c’ in B and C also shown as a diamond in C; hence, the unit was deemed to be “inhibited” relative to the pre-DBS interval. (D) The types of responses to DBS observed in the population of samples analyzed in this study. The symbols denote the pre ■, during • and post-stimulation intervals ◆, while the color indicates the type of response, blue – inhibition, red – activation, and black – no significant change. (For interpretation of the references to color in this figure legend, the reader is referred to the web version of this article.)

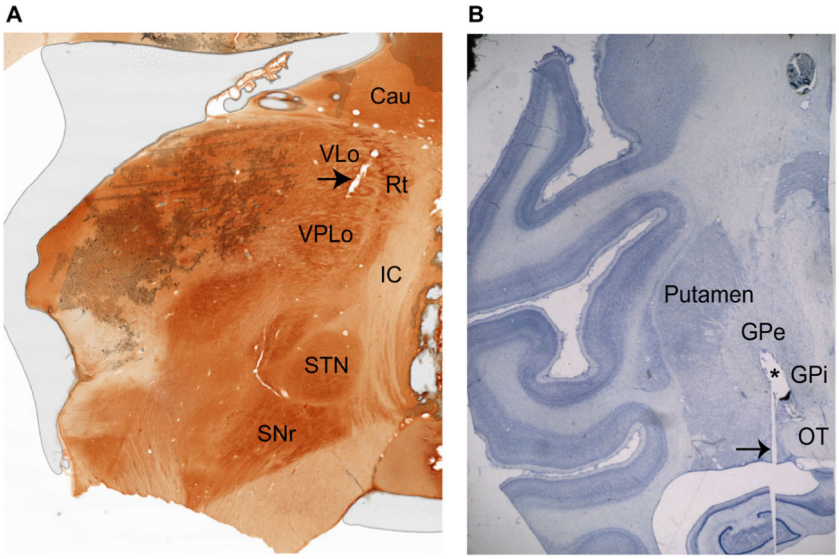

Figure 2.

Histological evidence for boundaries of VA/VLo and VPLo and DBS lead placement in the GPi. (A) Sagittal acetylcholinesterase stain shows the location of the thalamic sub-nuclei. The arrow indicates a recording track passing through the VLo. (B) Nissl stained coronal slice showing the location of the DBS lead (marked with an asterisk) passing through the pallidum. The histology image has been included here after obtaining permission from the publisher. The arrow points to an artifact in the slice preparation. The abbreviations are: Cau: caudate, IC: internal capsule, GPe: globus pallidus externus, GPi: globus pallidus internus, OT: optic tract, SNr: substantia nigra pars reticulate, STN: subthalamic nucleus, Rt: reticular thalamus, VLo: ventralis lateralis pars oralis, VPLo: ventralis posterior lateralis pars oralis.

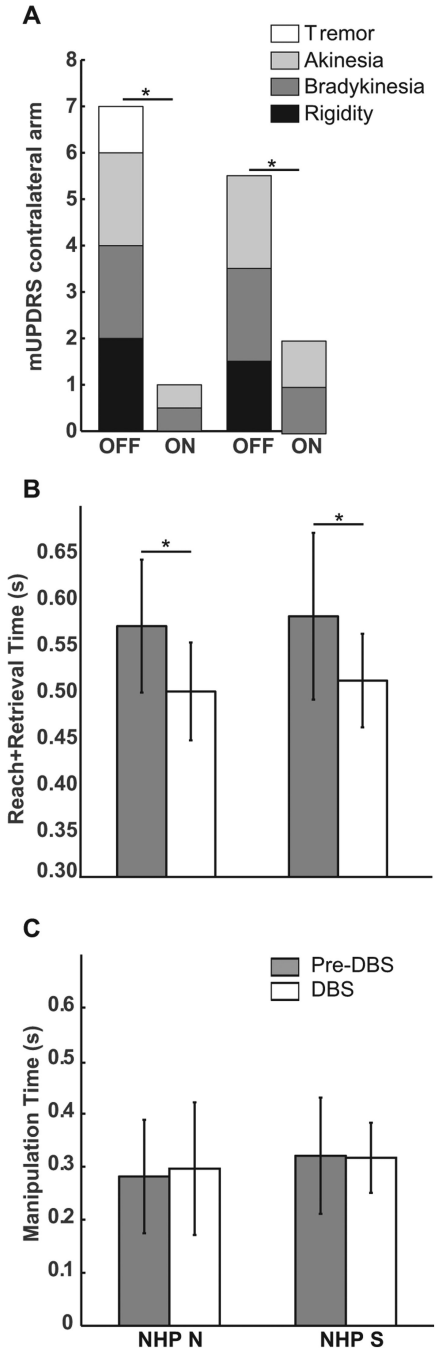

Figure 3.

GPi DBS improved parkinsonian motor signs. (A) Median composite subscale and cumulative scores for the affected upper extremity for Monkey N and Monkey S. In both animals, rigidity and tremor were completely resolved during GPi DBS, while akinesia and bradykinesia were reduced significantly. (B) GPi DBS significantly reduced the movement time (i.e. reach plus retrieval time) component of the Klüver board task. (C) Manipulation time was not significantly different between conditions (*$p < 0.05$). Error bars in B and C are one standard deviation from the mean. Abbreviation NHP stands for non-human primate.

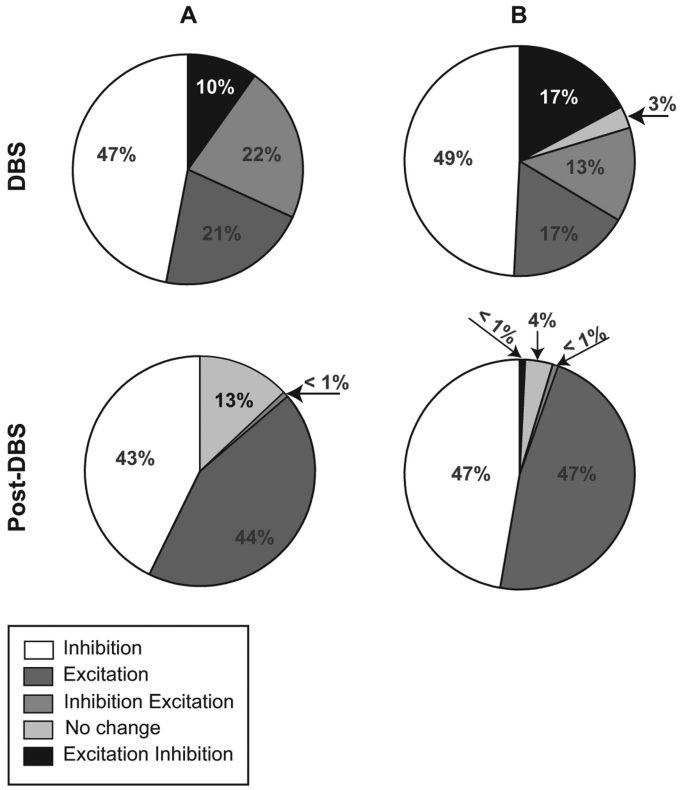

Figure 4.

A large proportion of the units in both nuclei were inhibited by GPi DBS. Distribution of the five different response types identified during (top row) and post (bottom row) GPi DBS: inhibition, excitation, inhibition-excitation, no change or excitation-inhibition for VA/VLo (A) and VPLo (B).

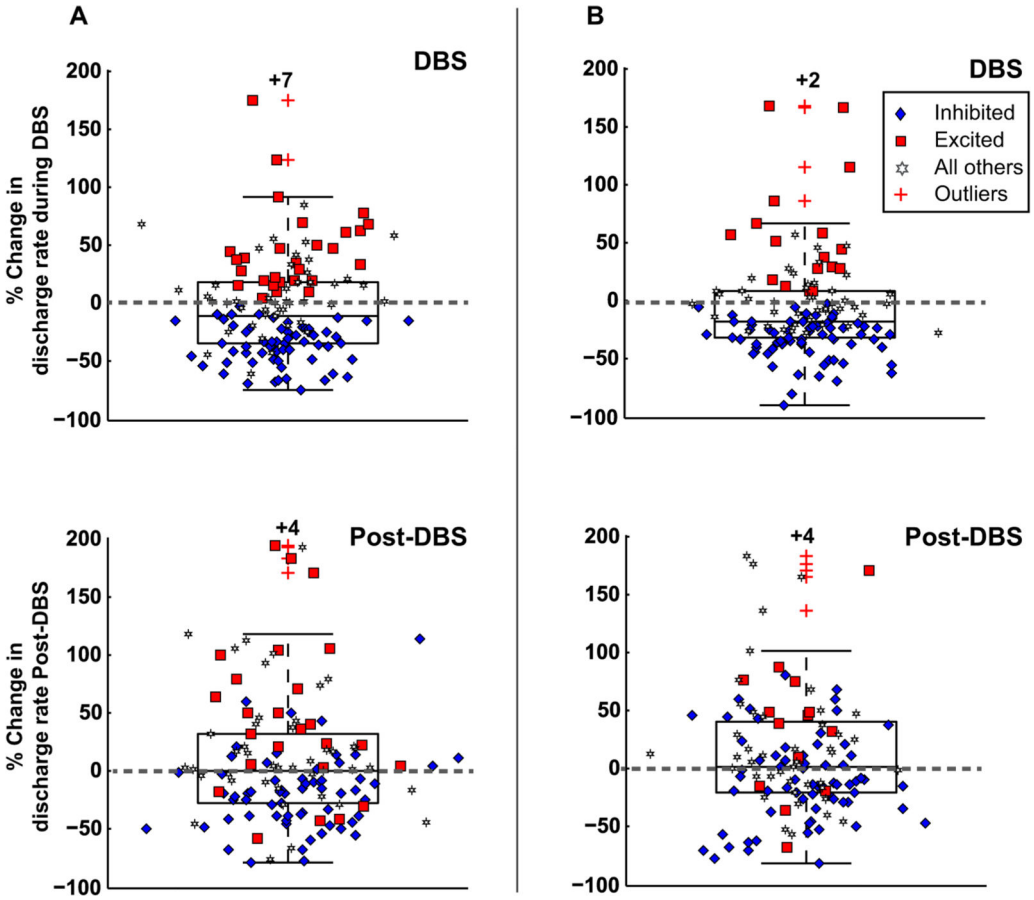

Figure 5.

The net discharge rate was reduced in both thalamic subnuclei during GPi DBS. Shown in the figure is the percent change in discharge rate during and post GPi DBS relative to the pre-DBS firing rate for VA/VLo (A) and VPLo (B) units; zero on the Y axis (gray dashed line) would indicate no change in the unit's discharge rate relative to the pre-DBS interval. The individual discharge rates (indicated by stars, diamonds and squares) were plotted with a random spread for clarity; classification of the units as inhibited (blue diamond), excited (red squares) or other (stars; includes EI, IE and NC response types). The box shows the 25th percentile, median and 75th percentile of the percentage change in discharge rate during- and post-DBS relative to the pre-stimulation interval. The red plus signs indicate outliers, those data points that are greater than the 75th percentile by more than 1.5 times the inter-quartile range. The numbers in black are the outliers that are not visible in the figure because the y-axis was scaled to improve the visibility of a majority of the data. (For interpretation of the references to color in this figure legend, the reader is referred to the web version of this article.)

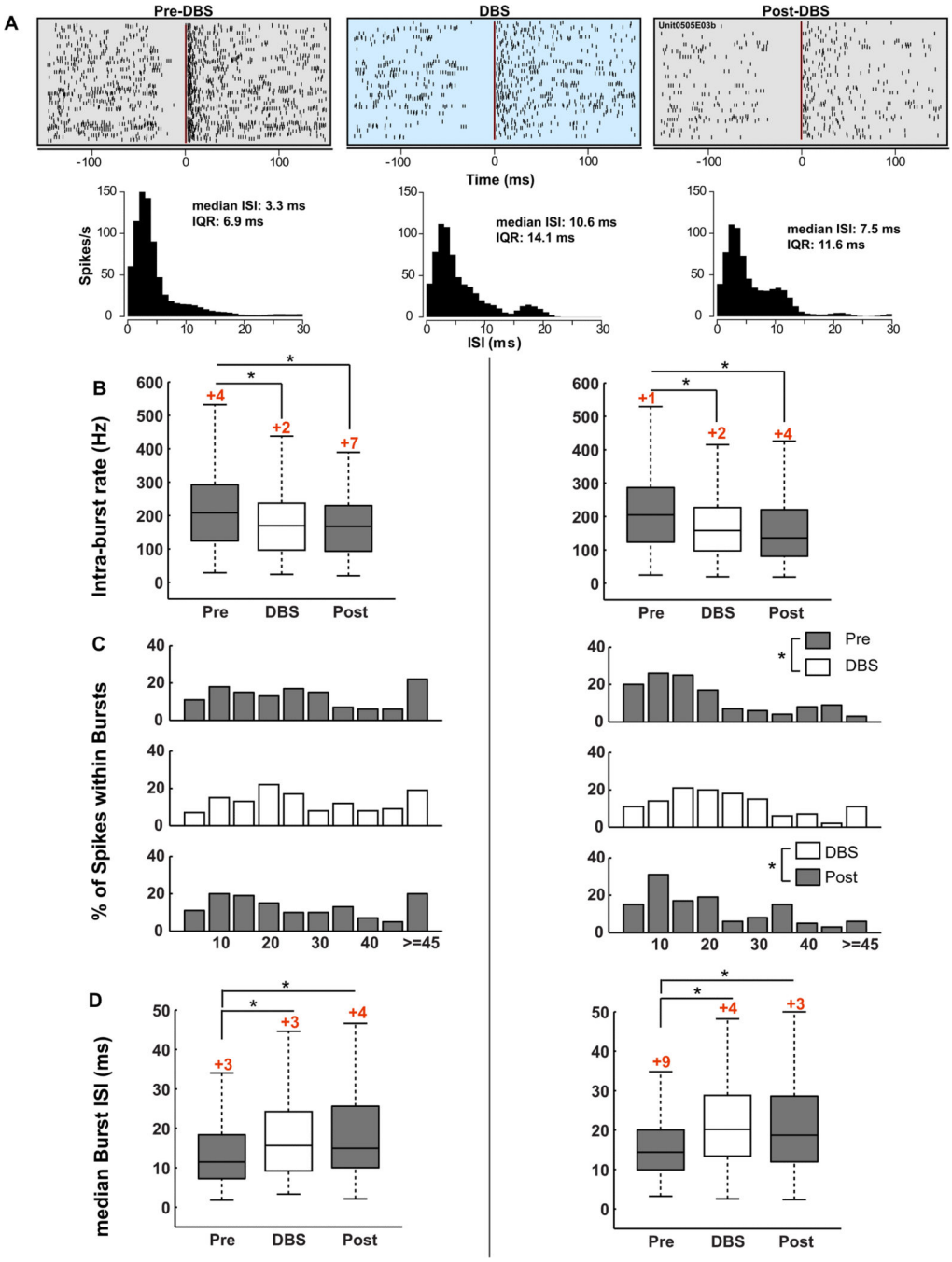

Figure 6.

The structure of bursts in the motor thalamus changed during GPi DBS. (A) Peri-burst raster plots demonstrating the effect of DBS on bursting activity; time zero is the beginning of a burst (one row per burst), as detected by the Poisson surprise method, and each vertical tick is the time occurrence of a spike, relative to burst onset. DBS reduces the bursting activity as can be seen by the more random and less clustered spike times in the during- and post-stimulation raters. This particular unit was recorded in the VPLo. Burst durations during the pre-, during- and post-stimulation intervals were 22.5, 39.9 and 37. 8 ms, respectively. The

median inter-spike interval and the spread (IQR: inter-quartile range) also increased during DBS and were sustained in the post-DBS phase. Mean intra-burst rate (B), percent of spikes within bursts (C) and median intra-burst, inter-spike interval (D) changed significantly during GPi-DBS (*$p < 0.05$). The numbers in red on top of the boxes, in A and C, indicate the outliers that are not visible because the y-axis was scaled to show the differences between pre, during and post stimulations in burst characteristics. (For interpretation of the references to color in this figure legend, the reader is referred to the web version of this article.)

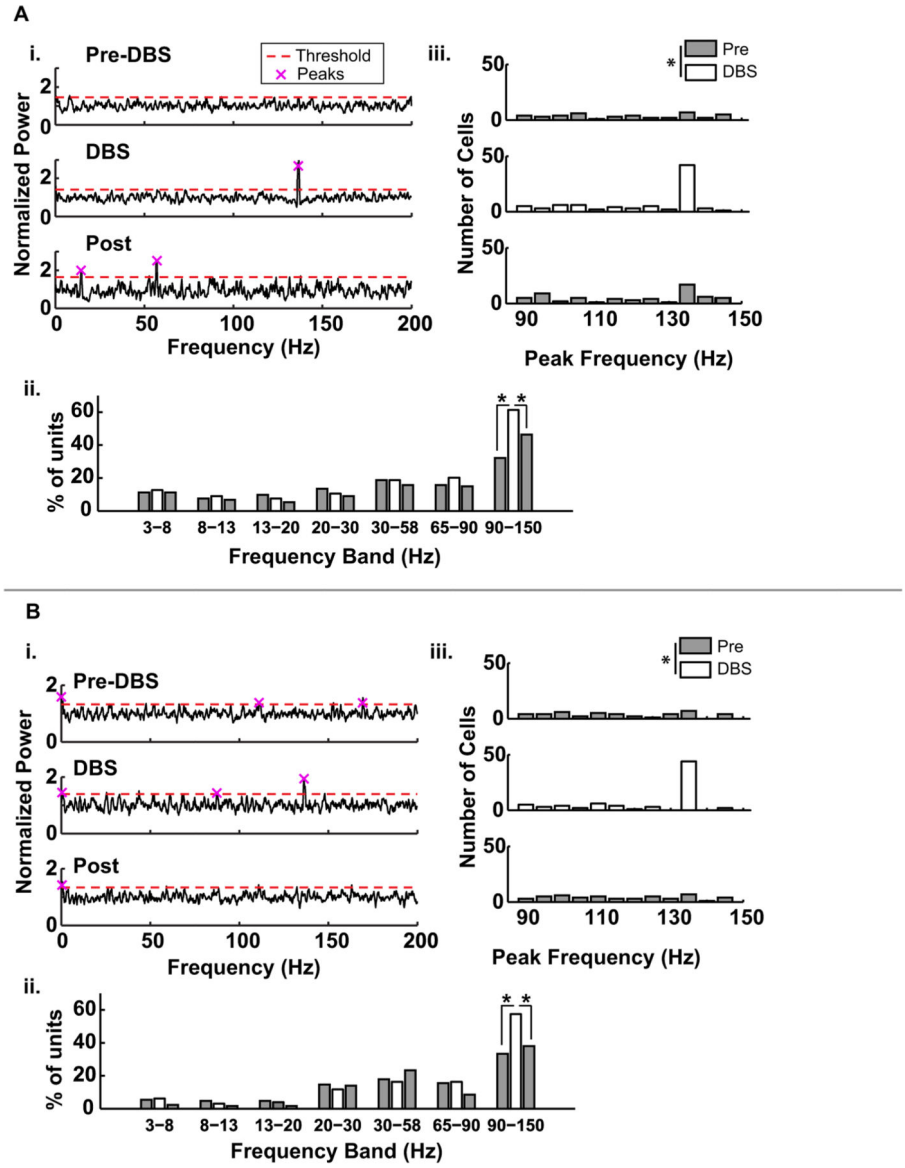

Figure 7.

A subset of units became entrained to the DBS frequency. (i) Example of power spectra before, during and post DBS; the power spectrum of the original spike train was normalized by the average spectra of a hundred shuffled spike trains. The pink 'X' indicates the peaks that were considered significant relative to the threshold (red dashed line); the threshold was defined as three standard deviations above the mean of the normalized spectrum in the 0.5–150 Hz range. (ii) Distribution of peak frequency in the 90–150 Hz band before, during and post DBS. (iii) Percent of units with oscillatory activity, in the 0.5–150 Hz band, in VA/VLo (A) and VPLo (B) nuclei during GPi-DBS (*$p < 0.05$). (For interpretation of the references to color in this figure legend, the reader is referred to the web version of this article.)

Table 1

Summary of neurons recorded from VA/VLo and VPLo.

Nucleus	NHP S				NHP N			
	Sites	Micro-stimulation response	Passive-movement response	Single units	Sites	Micro-stimulation response	Passive-movement response	Single units
VA/VLo	98	0	12	108	38	0	12	26
VPLo	108	108	60*	94	31	27	21	35

*The response of all isolated neurons to passive joint manipulation was assessed; however, a clear response was not observed in every case because the subjects resisted during the passive manipulation examination. Abbreviation NHP stands for non-human primate.

Table 2

Median and interquartile range for measures of bursting activity in the pre, during, and post DBS intervals.

Interval	VA/VLo					VPLo				
	IBR (Hz)	% Spikes within bursts	Burst duration (ms)	Burst frequency (Bursts/min)	Median ISI (ms)	IBR (Hz)	% Spikes within bursts	Burst duration (ms)	Burst frequency (Bursts/min)	Median ISI (ms)
Pre	208.2, 168.2	22.9, 25.6	46.0, 42.8	34.1, 36.6	11.5, 11.1	204.9, 163.5	12.4, 17.8	57.7, 43.4	21.8, 22.0	14.4, 10.1
DBS	169.3, 140.7	22.8, 24.3	58.6, 50.1	41.8, 48.3	15.6, 15.0	157.7, 129.8	18.8, 16.5	61.5, 49.7	29.1, 32.2	20.1, 13.7
Post	168.8, 135.2	19.6, 24.9	60.4, 60.4	36.8, 50.8	15.0, 15.6	135.6, 139.3	14.9, 21.9	63.2, 55.6	27.2, 34.1	18.7, 16.7

The abbreviation IBR stands for the average intra-burst rate.